NASA Technical Memorandum 82798

High-Speed Motion Picture Camera Experiments of Cavitation in Dynamically Loaded Journal Bearings

Bo O. Jacobson and Bernard J. Hamrock
Lewis Research Center
Cleveland, Ohio

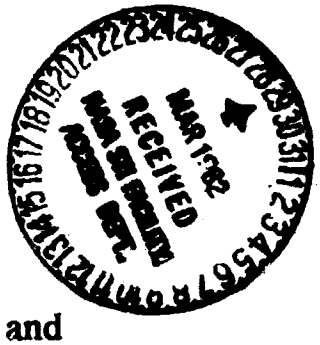

Prepared for the
Joint Lubrication Conference
cosponsored by the American Society of Mechanical Engineers and the American Society of Lubrication Engineers
Washington, D.C., October 5-7, 1982

NASA

HIGH-SPEED MOTION PICTURE CAMERA EXPERIMENTS OF CAVITATION IN DYNAMICALLY LOADED JOURNAL BEARINGS

Bo O. Jacobson and Bernard J. Hamrock

National Aeronautics and Space Administration
Lewis Research Center
Cleveland, Ohio

SUMMARY

It is important to know when and where cavitation occurs in bearings because cavitation has an effect on both the power loss and stability of the bearing. A bearing without cavitation can very well be unstable (vibrating) for the same working conditions where a cavitating bearing is stable. A high-speed camera was used to investigate cavitation in dynamically loaded journal bearings. The length-diameter ratio of the bearing, the speeds of the shaft and bearing, the surface material of the shaft, and the static and dynamic eccentricity of the bearing were varied. The results reveal not only the appearance of gas cavitation, but also the development of previously unsuspected vapor cavitation. Vapor cavitation is defined as cavitation where the cavitation bubbles contain mainly vapor, and gas cavitation is defined as cavitation where the cavitation bubbles contain mainly non-condensing gas. It was found that gas cavitation increases with time until, after many hundreds of pressure cycles, there is a constant amount of gas kept in the cavitation zone of the bearing. This gas can in some cases be transported through the high-pressure zone of the bearing without the cavitation bubbles collapsing. This means that the gas can have pressures of many times the atmospheric pressure. Vapor cavitation bubbles, on the other hand, collapse at pressures lower than the atmospheric pressure and cannot be transported through a high-pressure zone. Furthermore unlike gas cavitation the amount of vapor cavitation in a bearing does not increase with time. Analysis is given to support the experimental findings for both gas and vapor cavitation.

E-1137

INTRODUCTION

Cavitation is defined as the disruption of a continuous liquid phase by the emergence of gas or vapor. Understanding the cavitation phenomenon in bearings has been a challenge to tribologists ever since Osborne Reynolds first introduced the subject in his classical 1886 paper. The work in the early 1930's by Swift and Stieber went far in the development of our present understanding of cavitation. Swift (1932) working from stability considerations and Stieber (1933) from flow continuity studies arrived at the same boundary condition

$$\frac{\partial p}{\partial x} = 0, \qquad p = p_{cavity}$$

Cavity pressure often differs little from atmospheric pressure and is usually taken as such for the boundary condition. Dowson and Taylor (1975)

give an excellent review of the developments in the field of cavitation, beginning with the Swift-Stieber boundary condition and continuing to recent times.

The most common cavitation boundary condition for steadily loaded bearings has been the zero-pressure-gradient condition of Swift and Stieber. This condition results from the assumption of continuity of mass flow at the boundary between the cavitation zone and the liquid-filled regions under steady-state conditions. However, in many bearings dynamic loads cause changes in the local film thickness. and the problem of determining the appropriate boundary condition requires a condition other than zero pressure gradient at the boundary. The studies of Olsson (1965 and 1974) suggest that the usual steady-state condition, $p = dp/dx = 0$, is adequate for the dynamic situation if the cavitation boundary moves at a speed less than half the journal surface speed. However, if the cavitation boundary moves at a speed greater than half the journal surface speed, a more realistic formulation of the boundary condition has to be applied.

The work of Olsson (1974) assumes a dynamic condition of the bearing such that stable whirling is occurring. That is, his 180^0 bearing is stationary and the journal rotates with constant angular velocity while its center performs a circular motion concentric with the bearing center (compares to $\epsilon_s = 0$ in this investigation). In the present experimental work the whirling motion of the bearing was normally not concentric with the shaft, and therefore the instantaneous minimum film thickness varied both in size and location. This type of shaft and bearing movement is what can be expected when there are both gravitational and centrifugal forces acting on the shaft-bearing system, as is found in squeeze-film dampers.

Surface tension of the lubricant and the bearing surfaces is important for the formation of the cavitation zone and the single cavitation bubbles in such dynamically loaded bearings. Especially the finer structures of the cavitation zones are very much influenced by the surface tensions of the lubricant-bearing-shaft system.

SYMBOLS

A	area of flat surface of bubble
b	width of journal, m
C	circumference of bubble, m
c	radial clearance
D	diameter of shaft, m
d	dynamic eccentricity
e	static eccentricity
h	oil film thickness, m
I	moment of inertia, m^4
L	length of shaft, m
p	oil pressure, N/m^2
q	gas pressure, N/m^2
R	radius of bubble, m
T	surface tension, N/m
t	time, s; and thickness, m
Δt	temperature drop, °C
V	volume, m^3
v	collapse velocity, m/s

x coordinate, m
α film coefficient of heat transfer, $W/(m^2\ °C)$
β heat of evaporation, J/kg
γ location of minimum film thickness, deg
$\dot{\gamma}$ angular speed of minimum film thickness, s^{-1}
ϵ_d dynamic eccentricity ratio, d/c
ϵ_s static eccentricity ratio, e/c
κ polytropic exponent
ρ density, kg/m^3
ω angular velocity, 1/s

Subscripts:

0 atmospheric conditions

APPARATUS AND TEST PROCEDURE

The apparatus is shown in figure 1. The main parts are a shaft that can rotate around its own center (see fig. 2 for more details) and a bearing that can vibrate in a circular motion around a center. Both the location of the center of vibration and the amplitude of the vibration can vary. The rotating shaft is driven by a continuously variable-speed gear and a 2-kW electric motor. The motion of the bearing vibration is driven by a continuously variable-speed gear and a 0.75-kW electric motor. The speeds of the shaft and bearing can both vary between 0 and 600 rpm. The amplitude of the vibration is given by the dynamic eccentricity that is determined from the setting of the parts shown in figure 3. By rotating one part relative to the other it is possible to vary the dynamic eccentricity between 0 and 0.5 mm. Since the radial clearance is 0.5 mm, the ratio ϵ_d of the dynamic eccentricity to the radial clearance can be varied between 0 and 1. By moving the bearing relative to the shaft it is possible to vary the static eccentricity between 0 and 0.5 mm. Since the radial clearance is 0.5 mm, the ratio ϵ_s of the static eccentricity to the radial clearance can be varied between 0 and 1. To avoid contact between the shaft and the bearing, the following inequality must be satisfied:

$$\epsilon_s + \epsilon_d \leq 1$$

The surface roughness of the bearing and shaft surfaces was much smaller than the minimum film thickness except when $\epsilon_s + \epsilon_d = 1$. Then the minimum film thickness and the surface roughness were of the same order of magnitude during about 5 percent of each vibration cycle.

Figure 4 shows four positions of the shaft relative to the bearing for a dynamically loaded journal bearing. The static eccentricity ratio is set at 0.4, and the dynamic eccentricity ratio is set at 0.6. The direction of the dynamic eccentricity rotates 90° counterclockwise in going from (a) to (b), (b) to (c), and (c) to (d). In figure 4(a) the shaft and bearing are shown to be in contact. Figure 5 defines the amount of dimensionless minimum film thickness, its location, and its angular speed as a function of the position of the dynamic eccentricity. At $\omega_2 t = 0$ the dimensionless minimum film thickness and its location are arbitrarily chosen as zero. Figures 4 and 5 therefore show that the instantaneous minimum film thickness varies both in size and location.

Figure 6 shows the three different lengths of the rotating shafts used (90, 45, and 22.5 mm). Since the diameter of the shaft was 90 mm, the length-diameter ratios L/D of the shafts tested were 1, 0.5, and 0.25.

Two different shaft surface materials were used to investigate the influence of surface tension on pressure buildup and cavitation. The two shaft surface materials used were aluminum (as shown in fig. 6) and polytetrafluoroethylene (PTFE). The PTFE shafts were made of a 5-mm-thick PTFE tube pressfitted on the outside of an aluminum shaft. It was impossible to manufacture the shafts from solid PTFE because of the poor dimensional stability of PTFE. Even the pressfitted PTFE bushings had to be tested within a few hours of manufacturing in order to avoid significant dimensional changes.

When the bearing was vibrating, its centerline had to be parallel to the centerline of the rotating shaft. Figure 7 shows the special mechanism manufactured to accomplish this. It consisted of three plates each coupled together with four thin plates made from spring steel. The spring steel plates could easily be bent in the direction perpendicular to the plates but were very stiff in the horizontal planes of the plates ($I_1 = bt^3/12$, $I_2 = tb^3/12, \ldots, I_2/I_1 = (b/t)^2 = (60/0.5)^2 = 14\ 400$). Because of the symmetry of the mechanism the thick plates were always parallel to each other when the thin plates were bent, as long as they did not buckle.

The lubricant to the bearing was gravity fed from a can placed approximately 600 mm above the bearing. The lubricant passed from the can through a line and entered the bearing at the top left of the Plexiglas tube shown in figure 7. The leakage through the bearing was decreased by placing a stationary Plexiglas plate to form a small clearance between the plate and the end of the bearing. Figure 7 also shows the Plexiglas sleeve that enabled the cavitation to be seen.

Figure 8 shows the high-speed motion picture camera used for recording the experiments. The camera could take up to 11 000 frames per second with ordinary 16-mm motion picture film. In the experiments presented in this report the framing rates were 1000 and 2000 frames per second.

The lighting used in the experiments was a three-phase 10-kW mercury lamp, as shown in figure 8, and four 1-kW lamps. Tissue paper was positioned around the apparatus to avoid the sharp reflections of the light from the lamps on the bearing assembly. This arrangement decreased the light intensity a little but gave a very uniform light intensity over the whole bearing.

The following ranges of conditions were considered:

(1) Bearing length-diameter ratios of 1, 1/2, and 1/4
(2) Static eccentricity ratios $\epsilon_s = e/c$ of 0, 0.2, 0.4, 0.6, and 0.8
(3) Dynamic eccentricity ratios $\epsilon_d = d/c$ of 0, 0.2, 0.4, 0.6, and 0.8
(Note that $\epsilon_s + \epsilon_d \leq 1$ in order to avoid damage to the bearing.)
(4) Shaft and bearing speeds of 0 to 600 rpm
(5) Shaft surface materials of either aluminum or PTFE

Those situations that provided interesting cavitation patterns were among the 33 cases filmed. Fifty-six thousand frames of film were shot, with a total shooting time of less than 1 min.

EXPERIMENTAL RESULTS

Figures 9 to 13 each contain four frames from the high-speed films that show the development and disappearance of vapor cavitation. In parts (a) of these figures vapor cavitation is undeveloped, parts (b) and (c) show its development, and in parts (d) it has dissolved and disappeared. The bearings shown in figures 9 and 10 had aluminum surface shafts; those shown in figures 11 to 13 had PTFE surface shafts. Figures 9 and 11 are for length-diameter ratios of 1, figures 10 and 13 for L/D of 1/4, and figure 12 for an L/D of 1/2. The framing rate of the camera was 1000 frames per second. The dynamic eccentricity ratio ε_d was 0.6, the static eccentricity ratio ε_s was 0.4, the angular velocity of the shaft ω_1 was 2.51 rad/s (24 rpm), and the angular velocity of the dynamic eccentricity ω_2 was 62.8 rad/s (600 rpm). The time difference between parts (a) and (d) was typically less than 50 ms, which shows how rapidly the vapor cavitation bubbles disappeared.

The films show that not only is the usual type of mainly gas-filled cavitation bubbles found in dynamically loaded journal bearings but cavitation bubbles containing mainly oil vapor are also present. To the authors' knowledge, this has never been shown before. The two types of cavitation bubbles are quite different. When the cavitation bubbles contain mainly vapor, they are called vapor cavitation bubbles: and when they contain mainly noncondensing gas, they are called gas cavitation bubbles. The gas cavitation bubbles can survive even in the high-pressure region of the bearing for a long time (much more than one cycle of vibration). On the other hand, vapor cavitation bubbles dissolve and disappear in less than a hundredth of a cycle of vibration (less than a millisecond). Without a high-speed camera one would not be able to observe the vapor cavitation. Furthermore this type of cavitation can cause erosive wear of adjacent surfaces, and its presence in dynamically loaded journal bearings is therefore an important observation.

ANALYSIS OF GAS CAVITATION

Whereas the pressure in a vapor bubble is assumed to be constant, the pressure in a gas bubble increases rapidly as the volume of the bubble decreases, such that

$$q = q_0 \left(\frac{V_0}{V} \right)^{\kappa} \tag{1}$$

where κ for diatomic gas molecules is in the range $1 \leq \kappa \leq 1.4$. The term $\kappa = 1$ means isothermal compression and $\kappa = 1.4$ means adiabatic compression.

The transport of gas into and away from a bubble is a slow process, as can clearly be seen from cavitation films, where it often takes hundreds of vibrations before the cavitation pattern stabilizes.

Figure 14 is a sketch of a two-dimensional bubble where the bubble radius is large as compared with the film thickness. For equilibrium to be satisfied, the following must be true for the pressure p in the liquid and q in the gas:

$$(q - p)\, 2Rh - (4R + 2h)\, T = 0$$

but $4R >> 2h$. Therefore

$$q = p + \frac{2T}{h} \tag{2}$$

Substituting values for the dimensions of the gas bubble into equation (1), we can write

$$q = q_0\left(\frac{V_0}{V}\right)^{\kappa} = q_0\left(\frac{h_0\pi R_0^2}{h\pi R^2}\right)^{\kappa} = q_0\left(\frac{h_0 R_0^2}{hR^2}\right)^{\kappa} \tag{3}$$

Substituting equation (3) into equation (2) gives

$$p = q - \frac{2T}{h} = q_0\left(\frac{h_0 R_0^2}{hR^2}\right)^{\kappa} - \frac{2T}{h} \tag{4}$$

In typical journal bearings the film thickness h is of the order of 10^{-5} to 10^{-3} m, which means that the term

$$\frac{2T}{h} \approx \frac{2 \times 0.03}{10^{-5} \text{ to } 10^{-3}} = 6000 \text{ to } 60 \text{ N/m}^2$$

or

$$\frac{2T}{h} \approx 0.06 \text{ to } 0.0006 \text{ bar}$$

Because a typical range of pressure in a journal bearing is 10 to 1000 bars, the surface tension effect can be neglected in comparison with the hydrodynamic pressure. Therefore

$$p = q = q_0\left(\frac{h_0 R_0^2}{hR^2}\right)^{\kappa} \tag{5}$$

The possible pressure increase in the gas bubble lies between the isothermal and the adiabatic conditions. The exponent for the polytropic compression in the experiments is probably about $\kappa = 1.2$.

If a gas bubble is transported from the low-pressure zone into a high-pressure zone and the film thickness decreases to half the previous value at the same time as the pressure increases from 1 bar to 100 bars, the bubble size decreases from the original size in a polytropic case with $\kappa = 1.2$ to

$$\frac{R}{R_0} = \left(\frac{p_0}{p}\right)^{1/2\kappa}\left(\frac{h_0}{h}\right)^{1/2} = \left(\frac{1}{100}\right)^{1/2.4}\left(\frac{2}{1}\right)^{1/2} = 0.208$$

Thus air bubbles can be transported straight through the high-pressure zone without collapsing. This is to be contrasted with what was found for the vapor bubbles, which collapsed within milliseconds of formation.

ANALYSIS OF VAPOR CAVITATION

A simple model of the vapor cavitation behavior in dynamically loaded journal bearings is to assume the pressure to be constant during the collapse of the bubble. This is a good approximation if the bubble moves much more slowly than the molecules in the vapor so that the condensation can take place at the same speed as the movement of the boundary. When the bubble becomes small ($<10^{-6}$ m), the surface tension and the pressure increase in the bubble due to the temperature being elevated will almost cancel each other out. Thus even then the liquid pressure will be fairly constant.

The equation defining the collapse velocity of a vapor cavitation bubble is

$$v = \frac{\alpha}{\beta\rho}\Delta t \tag{6}$$

where

ρ density of saturated oil vapor for given temperature
α film coefficient of heat transfer for condensing oil steam at low (zero) flow velocity, $W/m^2\ ^\circ C$
β heat of evaporation for oil, J/kg
Δt temperature drop from vapor to liquid oil

Equation (6) is valid as long as all the condensation occurs on the moving surface.

If the bubble does not occupy the entire clearance space, condensation occurs completely around the bubble, as is indicated in the results presented, and adjustment to equation (6) is needed. When the flat cavitation bubble is collapsing, condensation also takes place at the flat surfaces. The collapse speed for circular bubbles when condensation takes place at the flat surface is

$$v = \frac{\alpha}{\beta\rho}\Delta t\,\frac{h + R}{h} \tag{7}$$

where

h oil film thickness
R radius of bubble

If instead of being circular the bubble is noncircular, the factor $(h + R)/h$ in equation (7) is changed as shown in equation (8)

$$v = \frac{\alpha}{\beta\rho} \Delta t \quad \frac{hC + 2A}{hC} \tag{8}$$

where

C circumference of flat surface of bubble
A area of flat surface of bubble

An order-of-magnitude estimate of the temperature drop from the vapor to the oil is given by the estimates of the vapor properties:

$$\rho = 6\times10^{-6}\ kg/m^3$$
$$\alpha = 600\ W/m^2\ ^\circ C$$
$$\beta = 350\ 000\ J/kg$$
$$v = 5\ m/s$$

$$\frac{(h + R)}{h} = \frac{(2\times10^{-5} + 5\times10^{-3})}{2\times10^{-5}} = 250$$

This gives a temperature drop of

$$\Delta t = 7.0\times10^{-5}\ ^\circ C$$

This means that the vapor bubble collapses almost without any resistance. In the films the initial size of the vapor cavitation region was typically 20 to 50 mm.

DISCUSSION OF RESULTS

For both aluminum surfaces and PTFE surfaces vapor cavitation as well as gas cavitation was found in the bearings. No conclusive difference in the size and form of the vapor cavitation region was found for materials with different surface tensions, but the fine inner structure within the vapor cavitation region was very different for different surface tensions of the bearing surfaces. The aluminum surface gave a vapor cavitation region consisting of small bubbles with thin walls of oil between them. The PTFE surface gave a vapor cavitation region consisting of one single big bubble.

CONCLUSIONS

The high-speed camera experiments of cavitation in dynamically loaded journal bearings revealed not only the appearance of gas cavitation, but also the development of previously unsuspected vapor cavitation. It was found that gas cavitation increases with time until, after normally many hundreds of pressure cycles, there is a constant amount of gas kept in the cavitation zone of the bearing. This gas can in some cases be transported through the high-pressure zone of the bearing without causing the cavitation bubbles to collapse. Thus the gas can have pressures of many times the atmospheric pressure. Vapor cavitation bubbles, on the other hand, collapse

at pressures lower than the atmospheric pressure and cannot be transported through a high-pressure zone. Furthermore unlike gas cavitation the amount of vapor cavitation in a bearing does not increase with time.

ACKNOWLEDGEMENTS

The authors are indebted to Luleå University, Sweden, the NASA Lewis Research Center, Cleveland, Ohio, and the National Research Council for their financial and technical support for this work.

REFERENCES

Dowson, D., and Taylor, C. M., "Fundamental Aspects of Cavitation in Bearings," Cavitation and Related Phenomena in Lubrication, Proceedings of the First Leeds-Lyon Symposium on Tribology, Mechanical Engineering Publication, London, 1975, pp. 15-26.

Olsson, K. O., "Cavitation of Dynamically Loaded Bearings," Chalmers Tekniska Högskolas Handlingar, No. 308, 1965, pp. 1-60.

Olsson, K. O., "Theoretical and Experimental Investigation of Pressure Buildup and Cavitation Regions in a Bearing with Stationary Whirl," Ph. D. Thesis Chalmers Tekniska Högskola, Gothenburg, Sweden, 1974.

Reynolds, O., "On the Theory of Lubrication and Its Application to Mr. Beauchamp Tower's Experiments, Including an Experimental Determination of the Viscosity of Olive Oil," Philosophical Transactions of the Royal Society, London, Vol. A177, 1886, pp. 157-234.

Stieber, W., Das Schwimmlager, Hydrodynamische Theorie des Gleitlagers, VDI-Verlag, Berlin, 1933.

Swift, H. W., "The Stability of Lubricating Films in Journal Bearings," Proceedings Institution of Civil Engineers, Vol. 23, No. 4809, 1932, pp. 267-88; Discussion pp. 289-322.

FIGURE CAPTIONS

Figure 1. - Test apparatus.

Figure 2. - Test shaft and motor.

Figure 3. - Dynamic eccentricity parts.

Figure 4. - Bearing geometries at four different times. $\epsilon_s = 0.4$; $\epsilon_d = 0.6$.

Figure 5. - Minimum film thickness, its location, and its angular speed as a function of time. $\epsilon_s = 0.4$; $\epsilon_d = 0.6$.

Figure 6. - Three lengths of rotating shafts used (90, 45, and 22.5 mm).

Figure 7. - Plexiglas sleeve and mechanism to keep bearing centerline parallel to centerline of rotating shaft.

Figure 8. - High-speed motion picture camera and lighting used in experiments.

Figure 9. - Cavitation in a dynamically loaded journal bearing for shaft with aluminum surface and L/D = 1.

Figure 10. - Cavitation in a dynamically loaded journal bearing for shaft with aluminum surface and L/D = 1/4.

Figure 11. - Cavitation in a dynamically loaded journal bearing for shaft with PTFE surface and L/D = 1.

Figure 12. - Cavitation in a dynamically loaded journal bearing for shaft with PTFE surface and L/D = 1/2.

Figure 13. - Cavitation in a dynamically loaded journal bearing for shaft with PTFE surface and L/D = 1/4.

Figure 14. - Sketch of two-dimensional cavitation bubble.

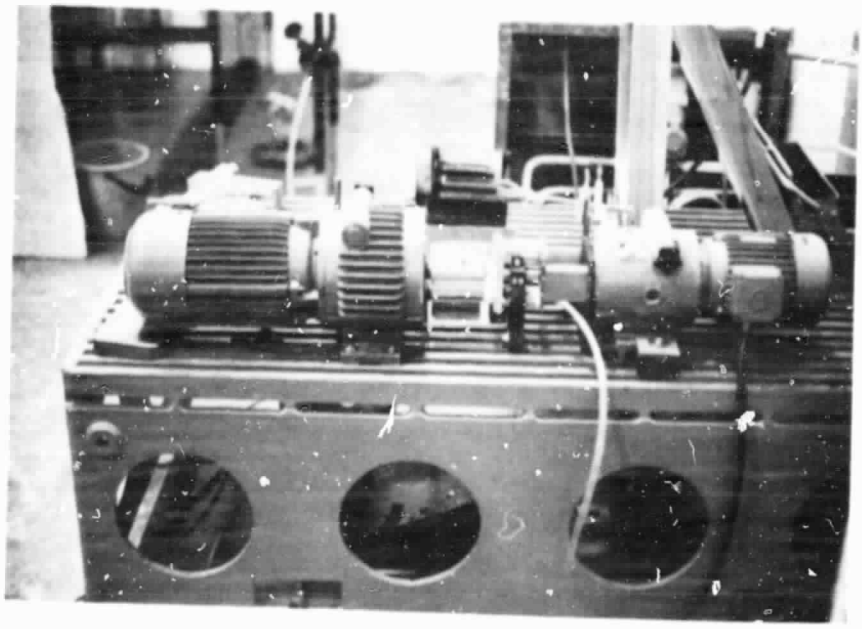

Figure 1. - Test apparatus.

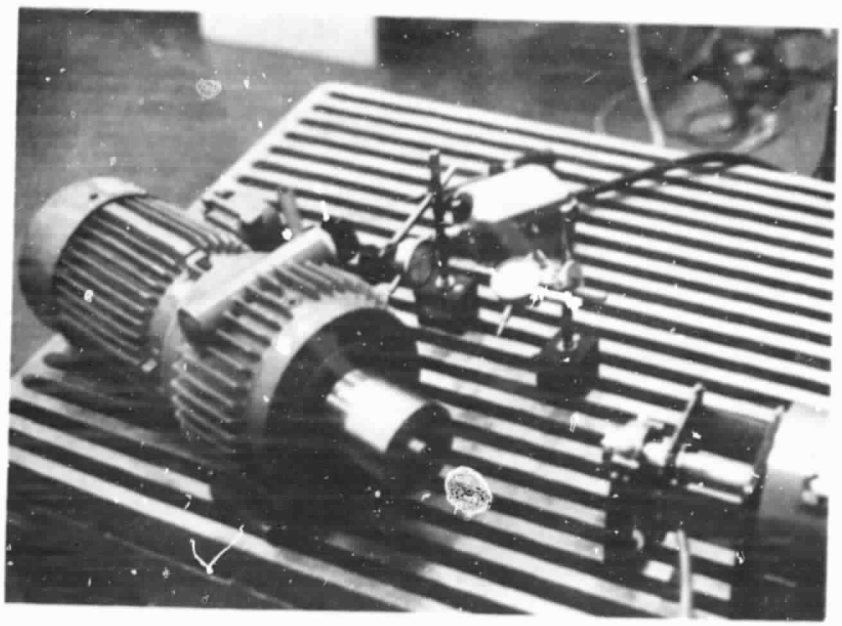

Figure 2. - Test shaft and motor.

Figure 3. - Dynamic eccentricity parts.

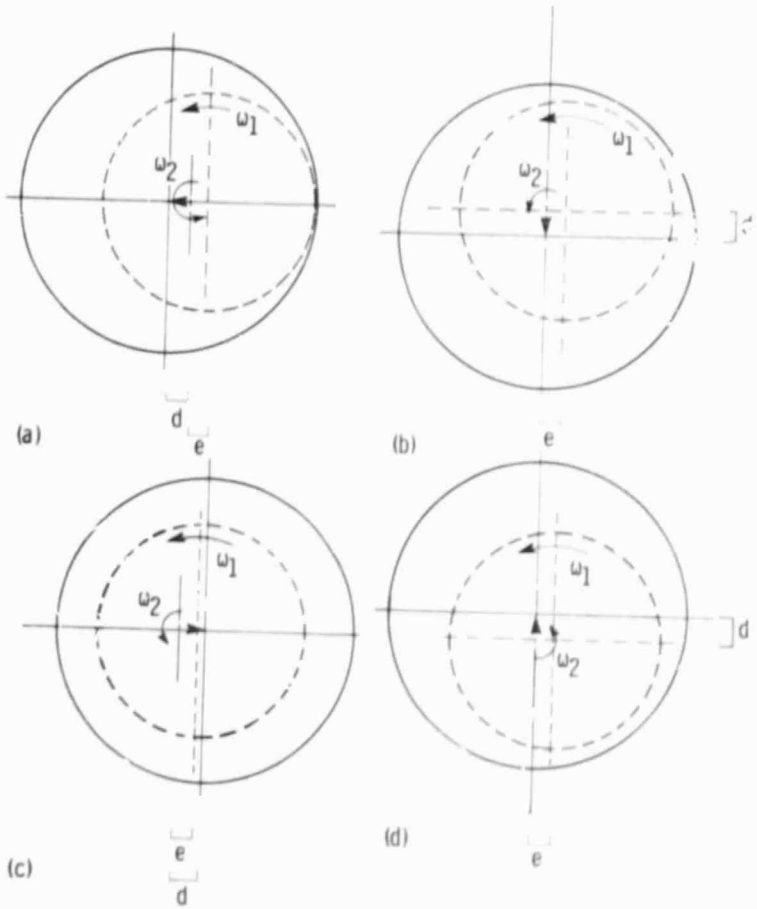

Figure 4. - Bearing geometries at four different times, $\varepsilon_s = 0.4$; $\varepsilon_d = 0.6$.

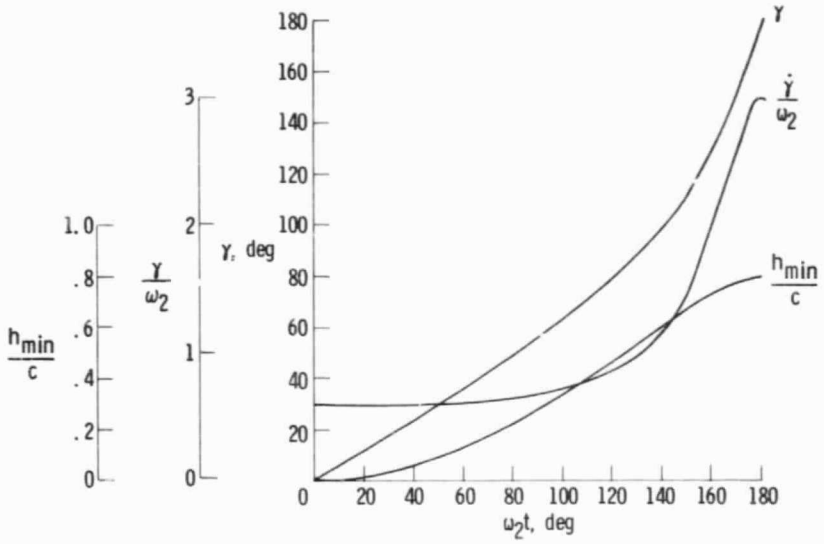

Figure 5. - Minimum film thickness, its location, and its angular speed as a function of position of dynamic eccentricity. $\epsilon_s = 0.4$; $\epsilon_d = 0.6$.

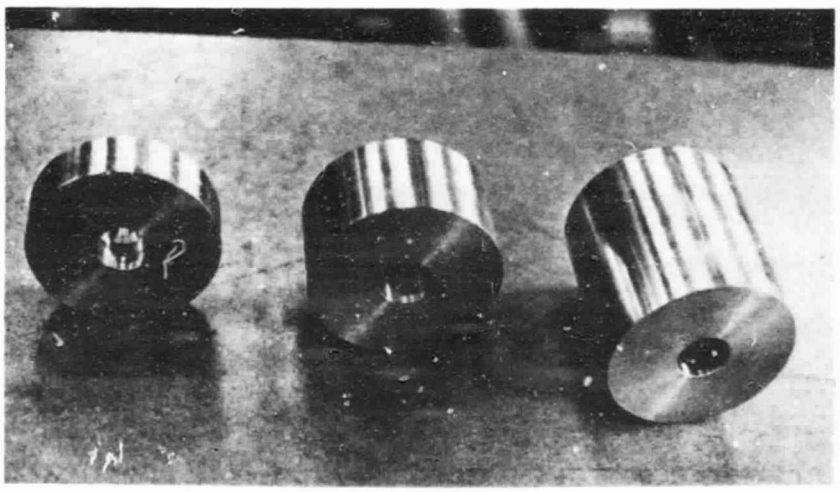

Figure 6. - Three lengths of rotating shafts used (90, 45, and 22.5 mm).

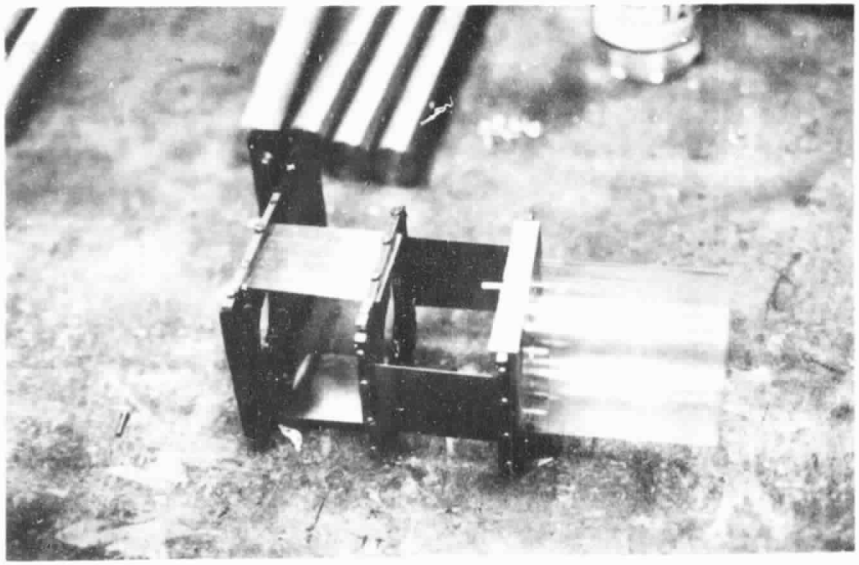

Figure 7. - Plexigas sleeve and mechanism to keep bearing centerline parallel to centerline of rotating shaft.

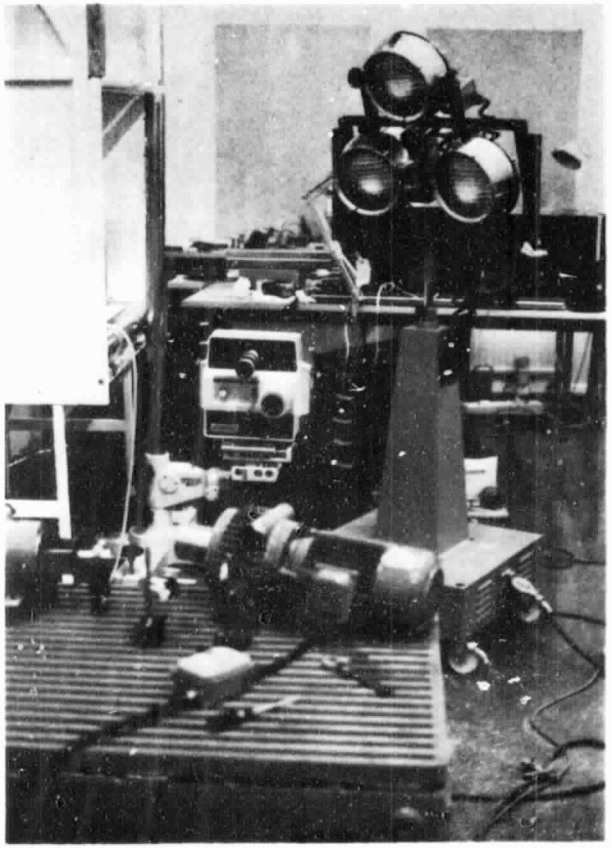

Figure 8. - High-speed motion picture camera and lighting used in experiments.

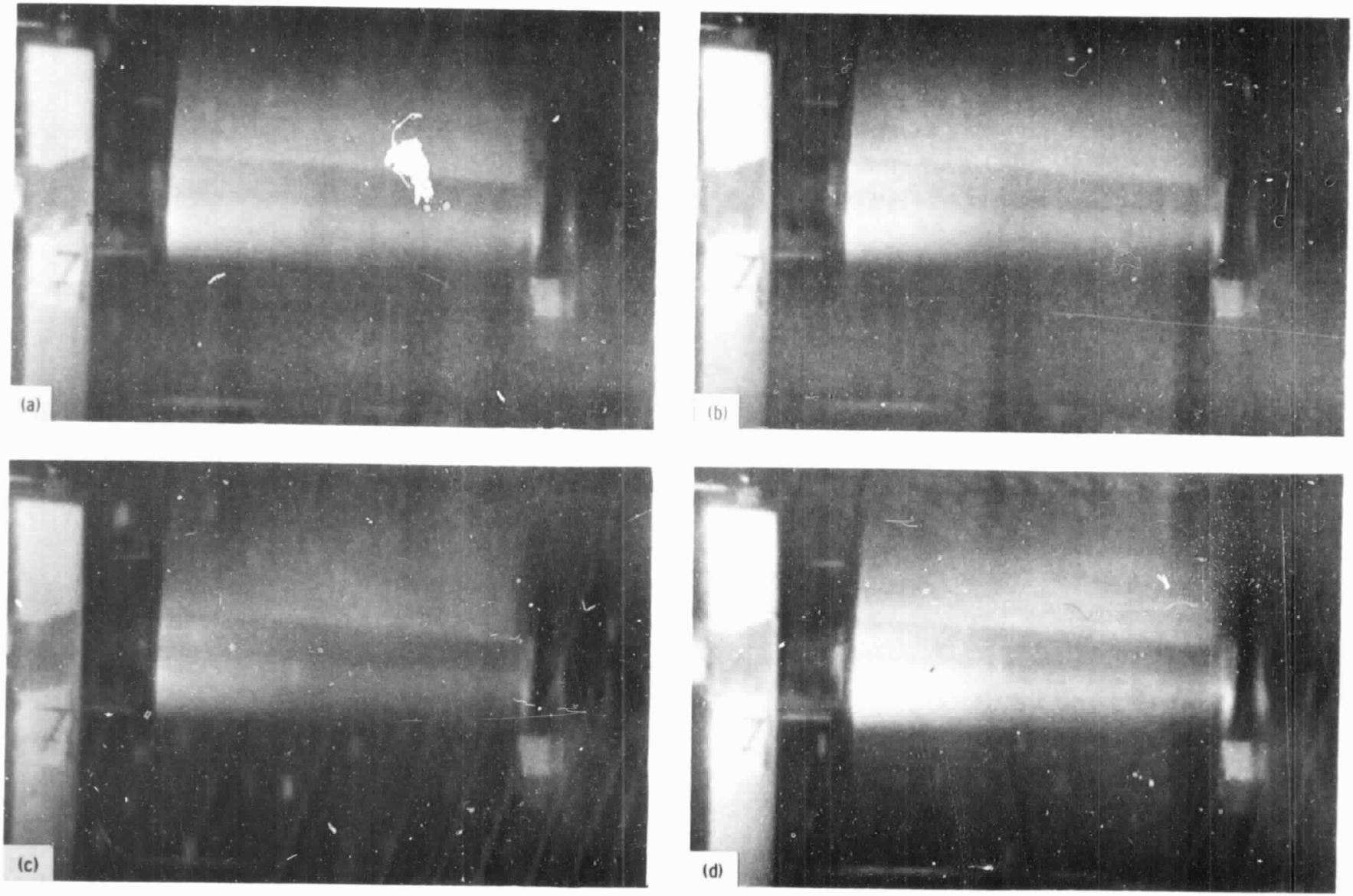

Figure 9. - Cavitation in a dynamically loaded journal bearing for shaft with aluminum surface and L/D = 1.

Figure 10. - Cavitation in a dynamically loaded journal bearing for shaft with aluminum surface and L/D = 1/4.

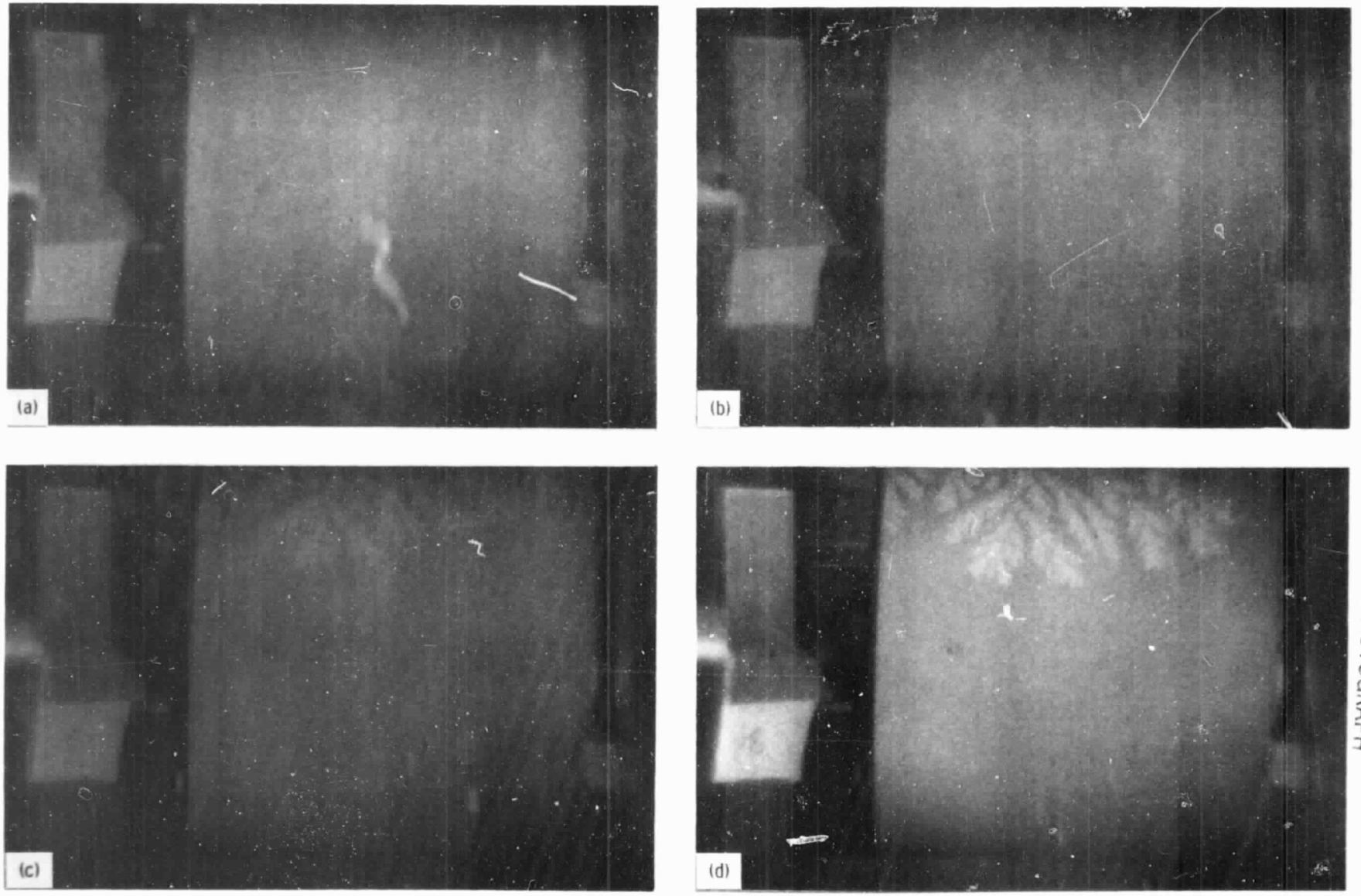

Figure 11. - Cavitation in a dynamically loaded journal bearing for shaft with PTFE surface and L/D = 1.

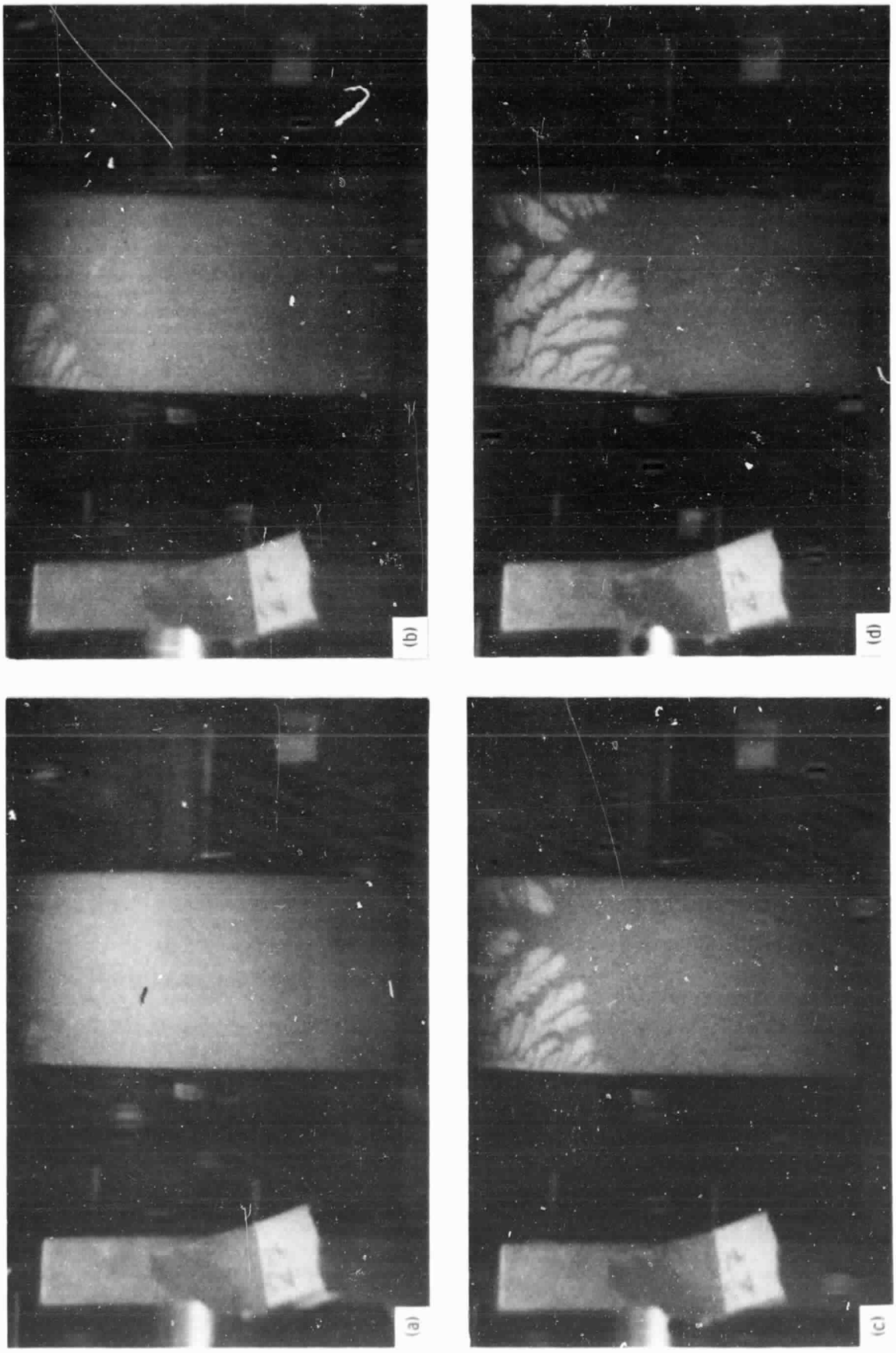

Figure 12. - Cavitation in a dynamically loaded journal bearing for shaft with PTFE surface and L/D = 1/2.

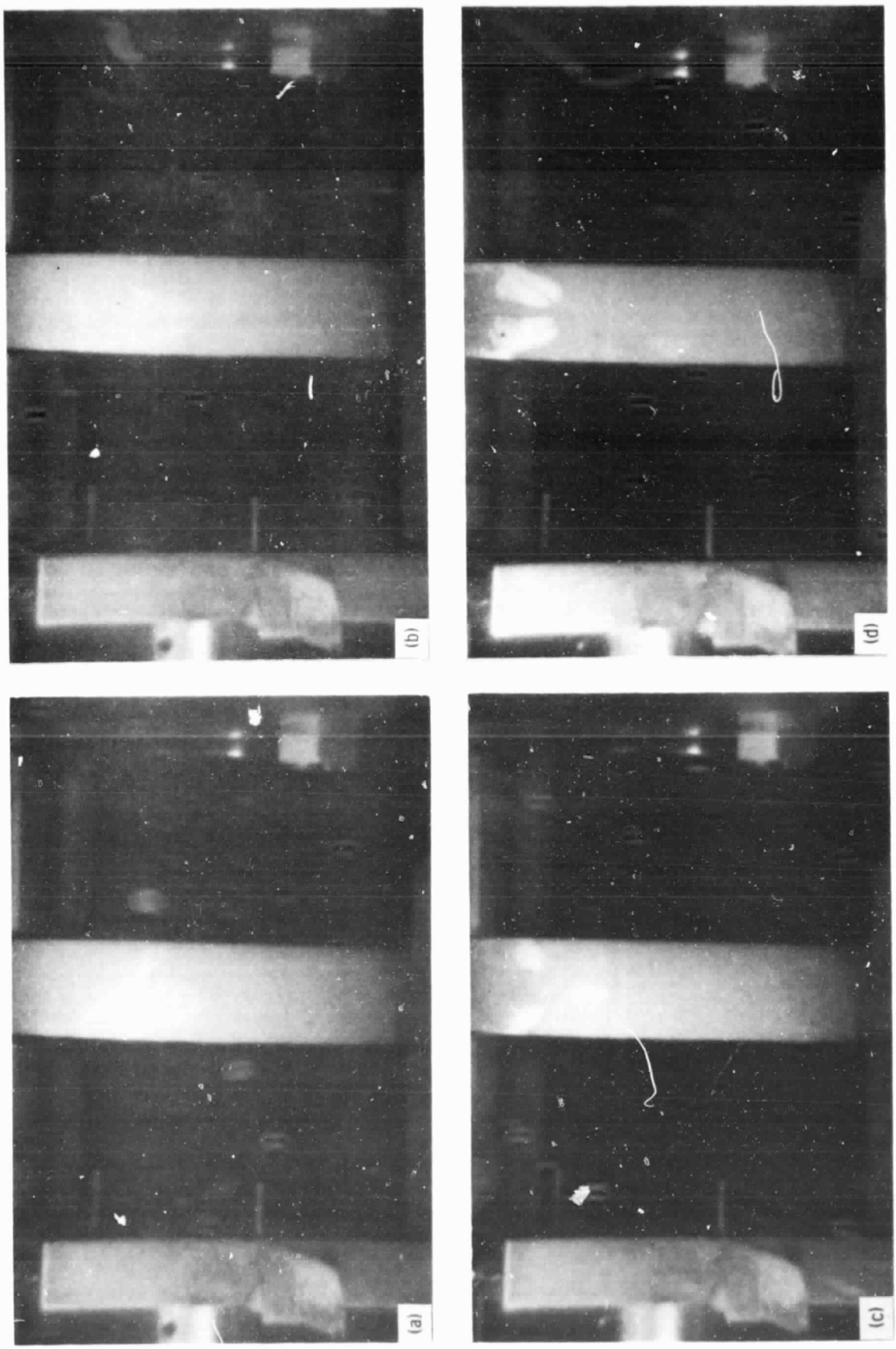

Figure 13. - Cavitation in a dynamically loaded journal bearing for shaft with PTFE surface and L/D = 1/4.

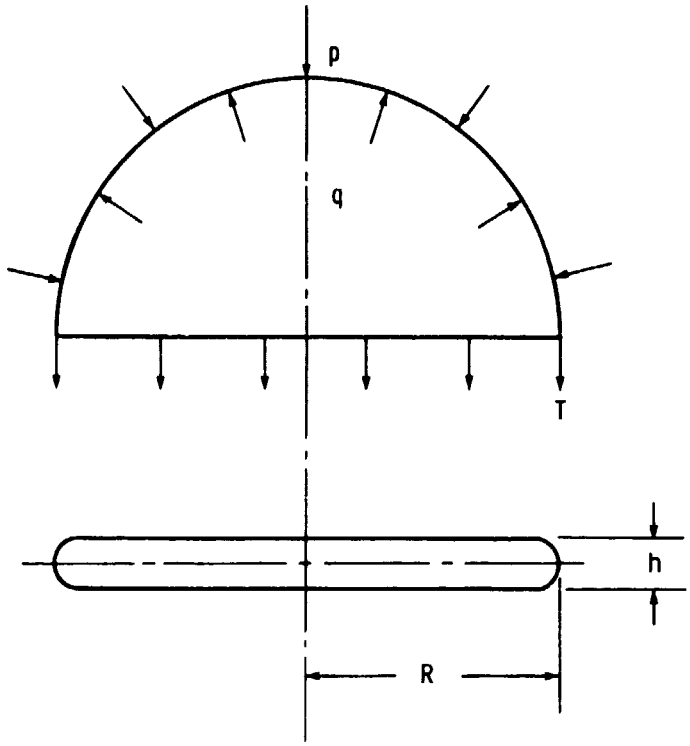

Figure 14. - Sketch of two-dimensional cavitation bubble.